Stabilization of Fast Pyrolysis Liquids from Biomass by Mild Catalytic Hydrotreatment: Model Compound Study

Depeng Han [1], Wang Yin [2], Ali Arslan [1], Tongrui Liu [1], Yan Zheng [1] and Shuqian Xia [1,*]

[1] Key Laboratory for Green Chemical Technology of State Education Ministry, School of Chemical Engineering and Technology, Tianjin University, Tianjin 300350, China; depengh@tju.edu.cn (D.H.); aliarslan@tju.edu.cn (A.A.); liutr1213@hotmail.com (T.L.); moirai0716@gmail.com (Y.Z.)

[2] Department of Chemical Engineering, ENTEG, University of Groningen, Nijenborgh 4, 9747 AG Groningen, The Netherlands; w.yin@rug.nl

* Correspondence: shuqianxia@tju.edu.cn; Tel.: +86-22-2740-6974

Abstract: Repolymerization is a huge problem in the storage and processing of biomass pyrolysis liquid (PL). Herein, to solve the problem of repolymerization, mild catalytic hydrotreatment of PL was conducted to convert unstable PL model compounds (hydroxyacetone, furfural, and phenol) into stable alcohols. An Ni/SiO$_2$ catalyst was synthesized by the deposition-precipitation method and used in a mild hydrotreatment process. The mild hydrotreatment of the single model compound was studied to determine the reaction pathways, which provided guidance for improving the selectivity of stable intermediate alcohols through the control of reaction conditions. More importantly, the mild hydrotreatment of mixed model compounds was evaluated to simulate the PL more factually. In addition, the effect of the interaction between hydroxyacetone, furfural, and phenol during the catalytic hydrotreatment was also explored. There was a strange phenomenon observed in that phenol was not converted in the initial stage of the hydrotreatment of mixed model compounds. Thermogravimetric analysis (TGA), Ultraviolet-Raman (UV-Raman), and Brunauer−Emmett−Teller (BET) characterization of catalysts used in the hydrotreatment of single and mixed model compounds demonstrated that this phenomenon did not mainly arise from the irreversible deactivation of catalysts caused by carbon deposition, but the competitive adsorption among hydroxyacetone, furfural, and phenol during the mild hydrotreatment of mixed model compounds.

Keywords: repolymerization; biomass pyrolysis liquid; mild catalytic hydrotreatment; mixed model compounds; competitive adsorption

1. Introduction

Pyrolysis liquids (PL), obtained from biomass fast pyrolysis, are considered potential liquid energy carriers for the production of renewable fuels and bio-based chemicals from lignocellulosic biomass [1]. They have a volumetric energy density that is 5 to 20 times higher than that of mother solid biomass [2], which favors storage and transport. The production of second-generation biofuels like bio-gasoline and bio-diesel from such biomass PL is of great interest and challenging for both academia and industry [3].

The composition of biomass PL is complex [4] and varies with the biomass feed [5]. Some components, such as aldehyde, ketones, carbohydrates, and phenols [6], are chemically and thermally unstable as the fast pyrolysis process occurs too rapidly to reach the equilibrium [7]. Worse still, organic acids in PL are corrosive and facilitate the polymerization of aldehydes, ketones, and carbohydrates under an elevated temperature [8–10]. All of the above undesired properties limit the use of PL as fuel or for bio-based chemical production [4].

Much effort has been devoted to increasing the stability of PL. The co-pyrolysis of biomass with other wastes, including plastic and tires, has been studied to obtain PL with a higher carbon and lower water content [11]. The catalytic upgrading of PL with an acid support like HZSM-5 and HY during pyrolysis has also been studied, in an attempt to increase the content of the aromatic hydrocarbon [12]. To reduce the total acid number, an alkaline catalyst like dolomite was used during the stabilization of PL [13]. Catalytic hydrogenation has been widely studied by researchers during the past 40 years [14,15] and is considered a promising technology for improving the undesired properties of biomass PL. The studies essentially show that it is difficult to produce transportation fuel or gasoline fractions by the one-step catalytic hydrogenation of PL at a high temperature (>300 °C) [16]. A two-stage upgrading process, including mild hydrogenation and high-temperature hydrodeoxygenation (HDO), was proposed by Baker and Elliott [9] in 1988, which was later widely accepted and studied by other researchers [7,10,17,18].

In the mild hydrogenation step, thermal liable components, especially aldehydes and ketones, are converted into corresponding alcohols and carbohydrates into sugar alcohols, which are more stable molecules and less prone to repolymerization. Additionally, the alcohols can be converted into hydrocarbons by HDO at a high temperature [19–21]. Generally, carbonyl-containing molecules and sugars are readily hydrogenated to corresponding alcohols, for example, glucose to sorbitol [22] and glycolaldehyde to ethylene glycol [23]. Meanwhile, the main parallel reactions, including acid-catalyzed reactions like sugar dehydration to furfural/5-HMF, further to humin-like molecules and condensation between aldehydes, ketones, and phenolics, predominate when poor mass transfer occurs due to viscous PL [24], especially when a continuous reactor configuration like a packed bed reactor with a large chunk of catalyst particles is applied [7]. The latter case reactions are detrimental to hydrogenation catalysts as increased Mw promotes coke/char formation on the catalyst surface, further blocking the porous structure of the catalysts [18,25], so it is essential to know the reactivity of various groups of compounds in PL, especially versus reaction temperatures, so that those molecules can be converted into more stable ones before repolymerization. Therefore, repolymerization reactions are suppressed to a low extent during mild catalytic hydrotreatment. Examples of recent research on the hydrotreatment of PL model compounds are summarized in Table S1. However, studies on the mild catalytic hydrotreatment of PL model compounds, especially mixed model compounds and the interactions among several models, are still scarce.

Here, we report the catalytic hydrotreatment of model compounds from a PL study using a home-made Ni/SiO$_2$ catalyst, in order to understand the behavior of compounds in PL during mild catalytic hydrotreatment. Compared to Ni-based catalysts, noble metal catalysts are much more expensive and traditional presulfided catalysts require the introduction of S into the system to maintain the activity, which will contaminate the products [8]. SiO$_2$ is a traditional inert material with a satisfactory thermal stability and has been commonly used as the support of catalysts in the hydrotreatment of PL and its model compounds [26]. Hydroxyacetone and furfural have previously been selected as model compounds because hydroxyacetone is an abundant molecule found in the aqueous phase of biomass fast pyrolysis liquids [27–30], and furfural is the dehydration product of carbohydrates and hard to handle compared to the mother C5 sugar, and has thus been used to mimic intermediates from sugar dehydration [31,32]. Phenol is also a component of PL [33], and has often been selected as the model compound in PL hydrodeoxygenation studies as the Ph-OH bond possesses the highest dissociation energy among the relevant phenolic C–O [34–38]. The aromatic ring is a possible precursor for polyaromatic formation, and will result in coke formation on the catalysts. To obtain insights into the conversion of the aromatic ring during the hydrotreatment process, simple phenol is selected as the model compound from PL. The reaction pathways are studied first, and the effects of temperature and initial hydrogen pressure are taken into account for the selectivity of stable alcohols, and thus inhibit the repolymerization tendency of the PL. More importantly, to simulate the biomass PL more factually, hydrotreatments of mixed model compounds at different mixing conditions are studied in detail. The suppression to hydroxyacetone and phenol conversion are discovered in

this process and an explanation of this phenomenon is given according to the reaction results and the characterization of the used catalyst.

2. Results and Discussion

2.1. Characterization of the Reduced Catalyst

2.1.1. Textural Properties and Elemental Composition

N_2 adsorption–desorption isotherms and pore distribution curves are illustrated in Figure 1 and the textural properties of Ni/SiO_2 and SiO_2 are shown in Table 1. As displayed in Figure 1, the presence of hysteresis loops indicated that the catalyst and its support contained mesoporous structures according to the IUPAC classification [39,40]. Furthermore, the type of hysteresis loop was changed from H3 to H1, which suggested that the pore size distribution became more uniform [39,40]. Besides, as shown in the pore distribution curves, mesopores of Ni/SiO_2 with a diameter range from 8 to 50 nm increased obviously compared with the SiO_2 support only, which was attributed to the formation of a new pore system comprised of nickel silicate or nickel hydroxide [41]. This result was in agreement with previous research [42]. As mesopores could reduce the diffusion resistance of reactant molecules that had contact with active components, this catalyst could be more active in the hydrotreatment of PL model compounds. In addition, the data in Table 1 further confirmed that the pore size and pore volume of the Ni/SiO_2 catalyst increased obviously, although the specific surface area decreased slightly. Furthermore, the inductively coupled plasma optical emission spectroscopy (ICP-OSE) analysis showed that the Ni/SiO_2 had an Ni content of 8.3 ± 0.3 wt %, as shown in Table 2.
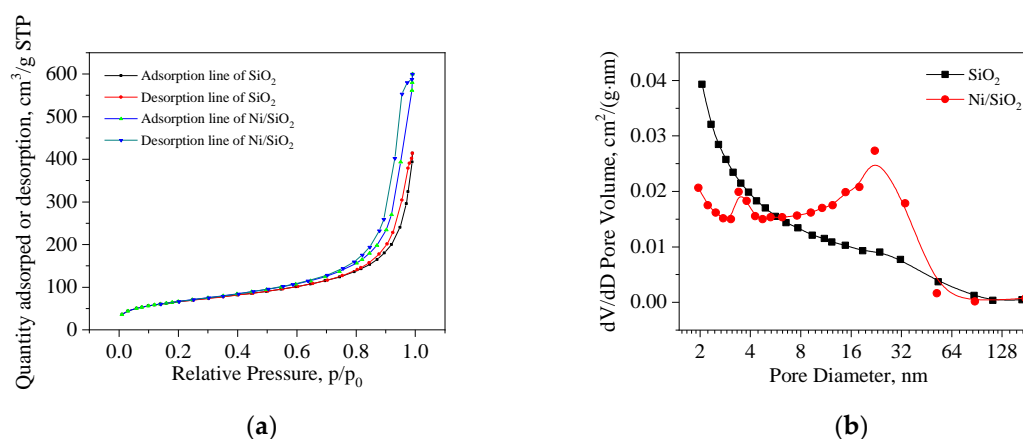

(**a**)   (**b**)

Figure 1. (**a**) N_2 adsorption–desorption isotherms and (**b**) pore distribution curves of SiO_2 and Ni/SiO_2.

Table 1. Textural properties of the support and catalyst.

Samples	S_{BET} [a], m^2/g	Pore Volume [b], cm^3/g	Average Pore Diameter [c], nm
SiO_2	226.6	0.6	14.3
Ni/SiO_2	218.2	0.9	19.2

[a] Brunauer−Emmett−Teller (BET) surface area. [b] Barret−Joyner−Halenda (BJH) desorption cumulative volume of pores between 1.700 and 300.000 nm in diameter. [c] BJH desorption average pore diameter (4V/A).

Table 2. Composition and particle size of the catalyst.

Sample	Ni loading [a], wt %	Ni Particle Size, nm	
Ni/SiO$_2$	8.3 ± 0.3	3.2 ± 1.6 [b]	3 [c]

[a] Ni loading was calculated by inductively coupled plasma optical emission spectroscopy (ICP-OES) analysis. [b]Ni particle size was obtained by a TEM image with more than 100 particles counted. [c] Ni particle size was evaluated by the Scherrer equation based on the Ni (111) plane in the XRD pattern.

2.1.2. H$_2$-Temperature Programmed Reduction (H$_2$-TPR)

The H$_2$-TPR profile of the calcined catalyst is displayed in Figure 2, and was rationally divided into three different peaks. The reduction peak at 223 °C can be attributed to aggregated NiO. Another peak at about 530 °C was associated with the well-crystallized NiO [43] or highly dispersed Ni species [42]. In addition, the main peak at 686 °C can be assigned to the reduction of nickel silicate or Ni^{2+} in the bulk silicate [42], which strengthened remarkably in intensity in comparison with the catalyst synthesized by incipient wetness impregnation [44]. This illustrated that the Ni/SiO$_2$ catalyst, which was prepared by the deposition-precipitation method, had a stronger metal-support interaction compared to the impregnation method. Additionally, the catalyst would process a better sintering resistance property and the active component loss could be prevented with a stronger metal-support interaction. Based on the H$_2$-TPR result of the catalyst, the reduction temperature for this catalyst was set to 700 °C.
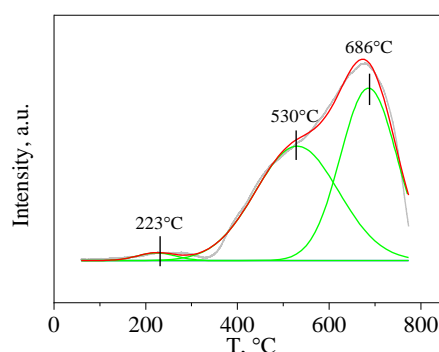

Figure 2. H$_2$-temperature programmed reduction (H$_2$-TPR) profile of the catalyst after calcination and the peak split results.

2.1.3. X-Ray Diffraction (XRD)

XRD patterns of the calcinated and reduced catalysts were obtained and are displayed in Figure 3. The characteristic diffraction peak at 2Theta = 21.98° was attributed to the SiO$_2$ support [26]. From the XRD pattern of the calcinated Ni/SiO$_2$ sample, the characteristic diffraction peaks situated at 2Theta = 34.00°, 35.67°, and 60.90° were attributed to the nickel silicate hydrate [45,46]. Therefore, XRD analysis further proved the formation of nickel silicate phase, which agreed with the TPR result in which the nickel silicate reduction peak was the main peak. However, for the reduced Ni/SiO$_2$ sample, the characteristic peaks, which were located at 2Theta = 44.51°, 51.85°, and 76.37°, corresponding to (111), (200), and (220) planes of Ni^0 phase, became obvious. This demonstrated that nickel silicate can be reduced into active Ni^0 species at 700 °C [47,48]. It could be observed that Ni^0 species exhibited a broader and weaker characteristic diffraction peak, which suggested that Ni^0 was highly dispersed on the SiO$_2$ support. Furthermore, the Ni^0 particle size was just 3 nm, as calculated by the Scherrer equation, and can be seen in Table 2. NiO, whose diffraction peaks were located at 2Theta = 43.29°, 37.25°, and 62.85°, may also be present in the catalyst system, which requires further characterization.
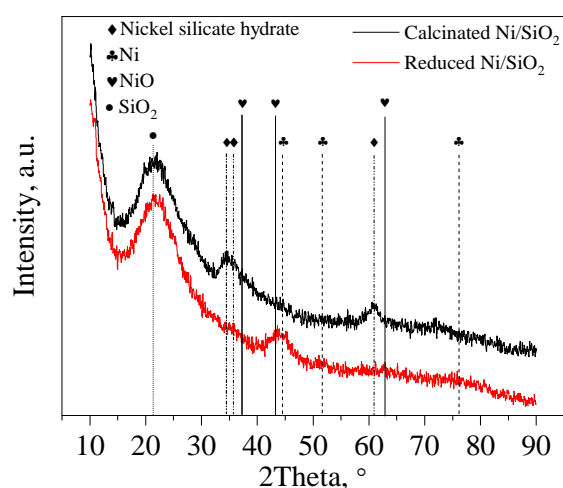
Figure 3. X-ray diffraction (XRD) patterns of calcinated and reduced catalysts.

2.1.4. X-Ray Photoelectron Spectroscopy (XPS)

Ni $2p^{3/2}$ XPS spectra of the calcinated and reduced Ni/SiO_2 samples were obtained and are exhibited in Figure A1. For the calcinated Ni/SiO_2 sample, the B.E. (binding energy) peak at around 856.5 eV can be attributed to the nickel silicate [49], which further confirmed the existence of nickel silicate phase. This result was consistent with previous XRD and TPR analysis. For the reduced Ni/SiO_2 sample, one peak at about 853.4 eV was related to Ni^0 after 700 °C reduction [50]. Another B.E. peak at 855.5 eV belonged to Ni^{2+} [51], with the satellite peak at the higher B.E. value. The appearance of NiO arose from the fact that Ni^0 particles on the surface of the reduced catalyst were reoxidized when exposed to air or passivated in 1% O_2/N_2 [52].

2.1.5. Transmission Electron Microscopy (TEM) and High-Resolution TEM (HRTEM)

TEM and HRTEM images of the reduced catalyst are exhibited in Figure 4. As shown in Figure 4a, Ni was uniformly dispersed on the catalyst surface. From the TEM statistical results presented it Figure 4a, it could be seen that the average particle size of Ni^0 was 3.22 ± 1.6 nm, which was counted based on more than 100 particles. This result was consistent with the XRD analysis, as presented in Table 2. Figure 4b shows that the lattice spacing is 0.2093 nm, which indicated that the Ni (111) crystalline plane was exposed [42].
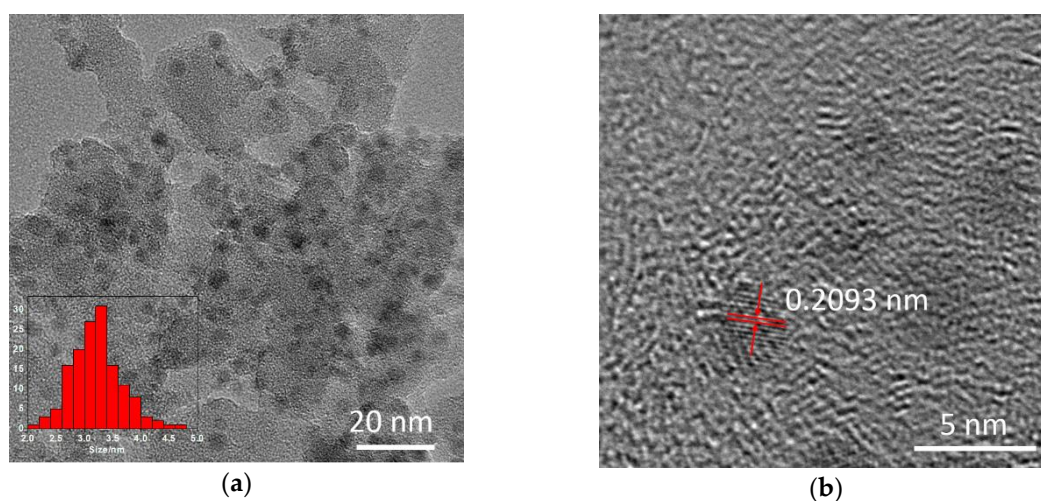

(**a**)

(**b**)

Figure 4. (**a**) Transmission Electron Microscopy (TEM) and (**b**) High-Resolution TEM (HRTEM) images of reduced Ni/SiO_2.

Therefore, the XRD and XPS characteristic results demonstrated that nickel silicate was generated on the Ni/SiO$_2$ catalyst, which was synthesized by the deposition-precipitation method. Subsequently, nickel silicate phase was reduced to active Ni^0 species at 700 °C, which was highly dispersed on the catalyst and possessed a narrow particle size distribution and smaller particle sizes. In addition, for the Ni/SiO$_2$ catalyst, the pore volume and average pore size increased in comparison with the pure SiO$_2$ support, which may reduce the diffusion resistance of model compounds to active component Ni^0.

2.2. Mild Catalytic Hydrogenation of Single Model Compounds

2.2.1. Reaction Pathway Analysis

The mild hydrotreatment of each single model compound was studied to determine their reaction pathways, which provided a footprint for further work on obtaining stable intermediates for "pure" pyrolysis liquid stabilization.

For the mild hydrotreatment of hydroxyacetone, 1,2-propanediol was the sole product, as was made evident by the quantitative selectivity, which did not vary when prolonging the reaction time and elevating the reaction temperature, as displayed in Figure 5. This result agreed with the research of Vispute and Huber [20], in which they prolonged the reaction time to 545 min at 175 °C and no obvious hydrogenolysis or dehydration/hydrogenation occurred. Our research further confirmed that almost no repolymerization occurred, even at a temperature as high as 240 °C, during the hydrotreatment of hydroxyacetone, as presented in in Figure 5C. It should be noted that, limited by the equipment, when the reaction temperature was set to between 150 and 250 °C, it took about 12 minutes for the temperature to reach the set point; that is, the conversion of the first 12 minutes happened during the heating process. The reaction pathway of the mild hydrotreatment of hydroxyacetone is illustrated in Scheme 1.
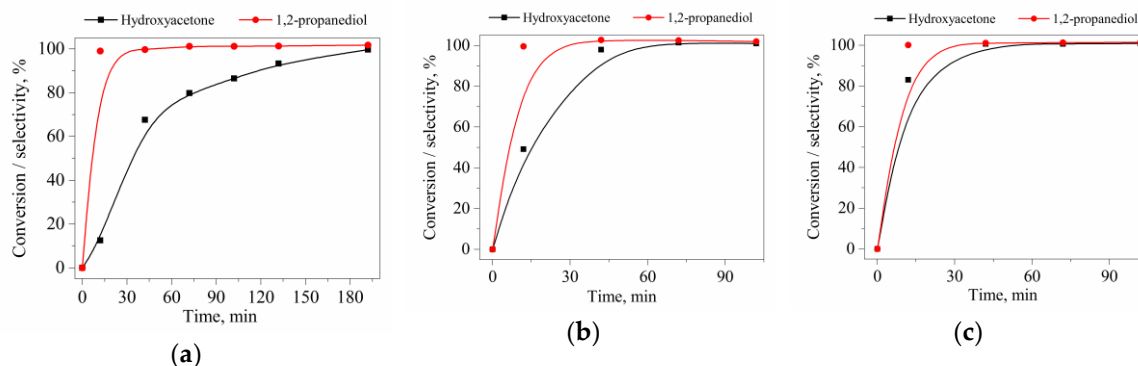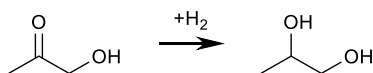

Figure 5. Effect of the reaction time on the conversion of hydroxyacetone and product selectivity of products at different temperatures ((**a**): 150 °C, 3.5 MPa; (**b**): 200 °C, 3.5 MPa; (**c**), 240 °C, 3.5 MPa).

Scheme 1. Reaction pathway of hydroxyacetone during catalytic hydrogenation.

Subsequently, the hydrotreatment of furfural was performed, and its conversion and the selectivities of products were plotted and are shown in Figure 6. As displayed in Figure 6a, the selectivity of furfuryl alcohol, which was the main product, decreased from 77.6% to 64.0% in the initial 30 min period. At the same time, the selectivities of the tetrahydrofurfuryl alcohol increased. This demonstrated that furfuryl alcohol was converted into tetrahydrofurfuryl alcohol. With prolongation of the reaction time, tetrahydrofuran, methyl furan, and methyltetrahydrofuran appeared after 180 min. As the reaction temperature was relatively low, the product that could not be quantified was mainly difurfuryl ether, according to the GC-MS results. As the selectivity of this part of the product

first increased and then decreased, it could be reasonably inferred that the difurfuryl ether initially formed could be decomposed into furfuryl alcohol and methyl furan that was further transformed into tetrahydrofuran and methyltetrahydrofuran.
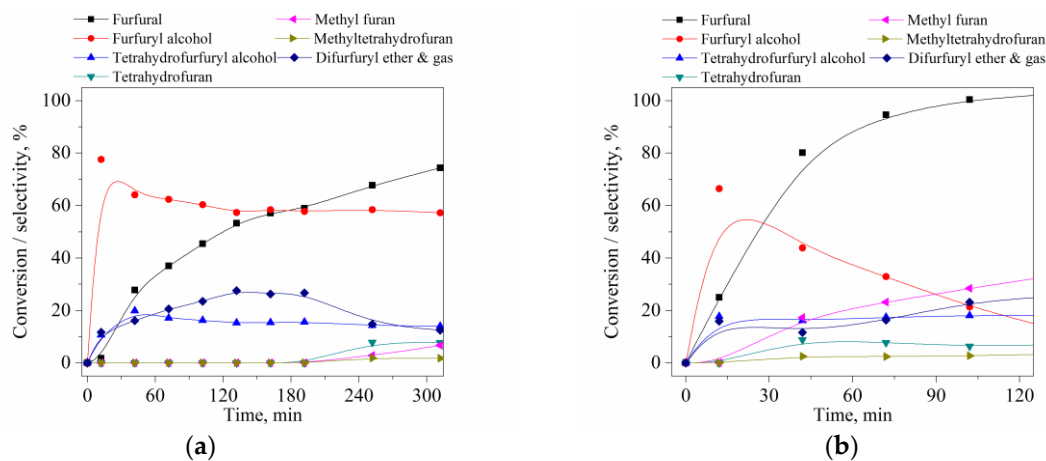

Figure 6. Effect of the reaction time on the conversion of furfural and the selectivities of products at different temperatures ((**a**): 150 °C, 3.5 MPa; (**b**): 200 °C, 3.5 MPa).

As displayed in Figure 6b, it was noted that the selectivity of furfuryl alcohol decreased rapidly from 66% to 13% within 120 min when the reaction temperature rose to 200 °C. At the same time, the selectivity of methyl furan increased to 33% and a small amount of other small molecular products may also have been generated [53]. This suggested that the dehydration/hydrogenation of furfuryl alcohol occurred and became more favorable at a higher temperature.

According to the above analysis and previous literature [54–56], the reaction pathway of the mild hydrotreatment of furfural is illustrated in Scheme 2. The solid arrows in Scheme 2 represent the main reactions, while the dashed ones represent the reactions that were more favorable at a higher temperature. Additionally, a higher temperature also favored the production of gas products, resulting in an increase of the other product selectivity. A detailed study on the effect of temperature was still necessary to achieve a higher selectivity of stable alcohols and avoid too much energy supply.
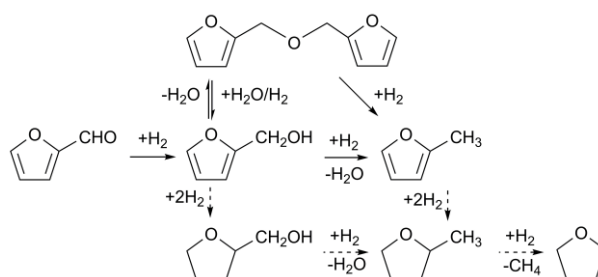
Scheme 2. Reaction pathway of furfural during catalytic hydrogenation.

The hydrotreatment of phenol was conducted and its conversion over time at different temperatures is shown in Figure 7. As shown in Figure 7a, the selectivity of cyclohexanone decreased from 87.7% to 10.7%. At the same time, the selectivity of cyclohexanol increased from 12.8% to 89.5%. This indicated that cyclohexanone could be converted into cyclohexanol with the prolonging of the reaction time during the mild hydrotreatment. However, when the temperature rose to 200 °C or even 250 °C, dehydration/hydrogenation of cyclohexanol to cyclohexane became obvious, according to Figure 7b,c.
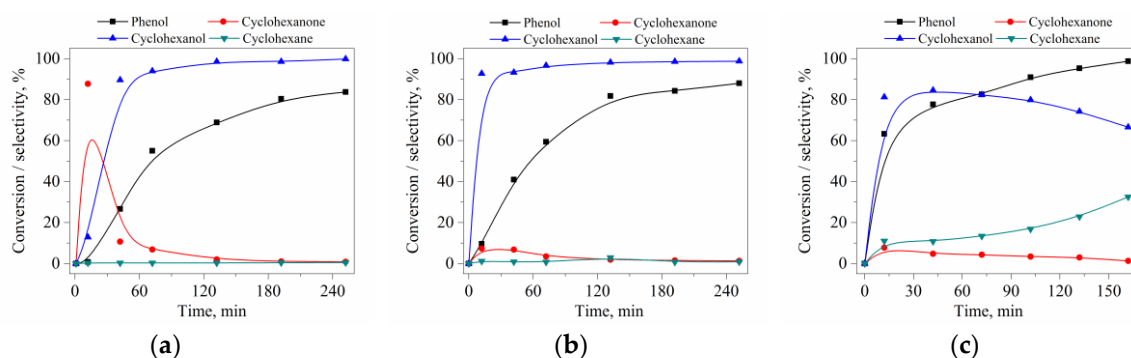
Figure 7. Effect of the reaction time on the conversion of phenol and the selectivities of products at different temperatures ((**a**): 150 °C, 3.5 MPa; (**b**): 200 °C, 3.5 MPa; (**c**): 250 °C, 3.5 MPa).

Based on the above analysis and previous literature [37,57,58], the reaction pathway of the mild hydrotreatment of phenol is presented in Scheme 3. The solid arrows represent the reactions at a low temperature, especially the stabilization of fast pyrolysis liquids, and the dashed one represents hydrodeoxygenation reactions at a high temperature when aiming for fully deoxygenated products like gasoline and diesel from pyrolysis liquids.
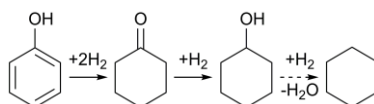
Scheme 3. Reaction pathway of phenol during catalytic hydrogenation.

2.2.2. Reaction Parameter Optimization for Improving the Stable Alcohol Selectivity

As a relatively high alcohol selectivity of a product can effectively resolve the problem of repolymerization in the storage and processing of PL, the temperature and initial hydrogen pressure were further studied in detail to increase the selectivity of stable alcohols and inhibit the dehydration/hydrogenation and hydrogenolysis reactions.

Figure 8a and Table S2 suggested the effects of temperature on the mild hydrotreatment of hydroxyacetone. It could be found that temperature had profound effects on the hydrogenation rate of hydroxyacetone, but almost no impact on the selectivity of 1,2-propanediol. It could be shown that no polymerization product was produced during the catalytic hydrotreatment of hydroxyacetone according to the product selectivity, which was almost 100%. In order to maintain a high conversion rate of hydroxyacetone, the temperature should be above 180 °C.
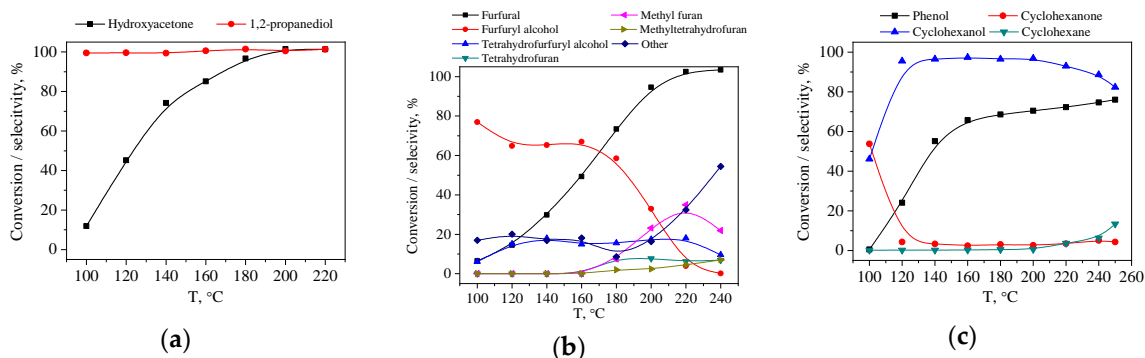

Figure 8. Effects of temperature on the conversion and product selectivities ((**a**): hydroxyacetone, 3.5 MPa, 1 h; (**b**): furfural, 3.5 MPa, 1 h; (**c**): phenol, 3.5 MPa, 1 h).

Figure 8b and Table S3 suggested the effects of temperature on the mild hydrotreatment of furfural. It can be observed that the products of the mild hydrotreatment of furfural were complicated. In addition, Scheme 2 indicated that furfuryl alcohol and tetrahydrofurfuryl alcohol were the desired products, which were stable and could not be repolymerized. However, the studies in the previous part suggested that the dehydration/hydrogenation of furfuryl alcohol was a major problem at a high temperature in the hydrotreatment of furfural. Therefore, to maintain the higher yield of stable furfuryl alcohol and tetrahydrofurfuryl alcohol and higher conversion of furfural, the temperature should be kept within a range from 160 to 200 °C, according to Table S3.

Figure 8c and Table S4 suggested the effects of temperature on the mild hydrotreatment of phenol. It could be noted that the selectivity of cyclohexanol was more than 95% in Figure 8C when the temperature was above 120 °C. However, previous studies have indicated that the dehydration/hydrogenation of cyclohexanol to cyclohexane was promoted when the temperature was higher than 200 °C. Therefore, in order to obtain a higher stable alcohol yield and supply a higher conversion of phenol, the reaction temperature should be controlled at about 200 °C.

The catalytic hydrotreatment of biomass PL involved vapor, liquid, and solid phases. Mass transfer played an important role in this process, especially for the reactions requiring hydrogen, including hydrogenation, hydrogenolysis, and dehydration/hydrogenation. Therefore, the effects of initial hydrogen pressure on the hydrotreatment of model compounds were studied in detail.

Figure 9 and Tables S5–S7 illustrated the effects of the initial hydrogen pressure on the conversion of model compounds and the selectivities of the products in the mild hydrotreatment of single model compounds. The conversion of three model compounds increased with the increase of the initial hydrogen pressure, but the selectivities of the desired products did not almost vary. The rule was consistent, no matter the mild hydrotreatment of hydroxyacetone, furfural, or phenol. In order to obtain a higher conversion of three model compounds and reduce the economic cost of excessive hydrogen consumption, the medium hydrogen partial pressure was satisfactory and was kept in a range of 3 to 4 MPa.
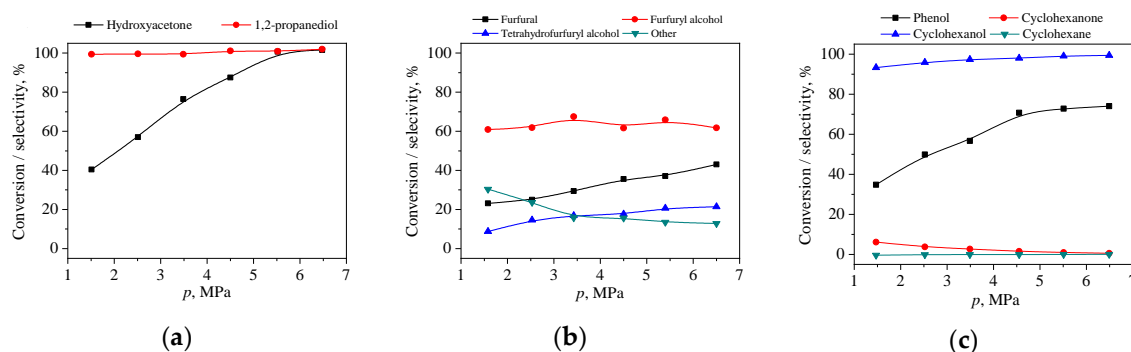

Figure 9. Effect of pressure on the conversion and product selectivity ((**a**): hydroxyacetone, 150 °C, 1 h; (**b**): furfural, 150 °C, 1 h; (**c**): phenol, 150 °C, 1 h).

Therefore, the temperature had a significant influence on the conversion of model compounds and the selectivities of stable alcohols. However, the initial hydrogen pressure affected only the conversion of model compounds, but hardly the selectivities of stable alcohols. According to the reaction parameter analysis of the hydrotreatment of the single model compound, it could be roughly inferred that the reaction parameters of the mild catalytic hydrotreatment of mixed model compounds were 180–200 °C and 3–4 MPa initial hydrogen pressure.

2.3. Mild Catalytic Hydrotreatment of Mixed Model Compounds

2.3.1. The Effect of the Interaction among Mixed Model Compounds in Hydrotreatment

In order to simulate the reaction of biomass PL more factually, the hydrotreatment of mixed model compounds of the three substances mentioned above was evaluated. At the same time, the effects of the interactions among hydroxyacetone, furfural, and phenol during the catalytic hydrotreatment of them could also be explored.

As discussed above, the catalytic hydrogenation of a single model compound of hydroxyacetone, furfural, and phenol, could obtain a satisfactory selectivity of stable alcohols as far as possible at 180 °C and 3.5 MPa initial hydrogen pressure. Firstly, the treatment of mixed model compounds was conducted under this condition (180 °C and 3.5 MPa initial hydrogen pressure) for 60 min. The results are exhibited in Figure 10. However, it can be seen that during the hydrotreatment of model compounds mixed by the three substances, the conversion of hydroxyacetone and phenol, especially the conversion of phenol, was almost inhibited. In order to explore the effects of the interactions among the three model compounds, the catalytic hydrotreatment processes of them at different temperatures and reaction times were studied.
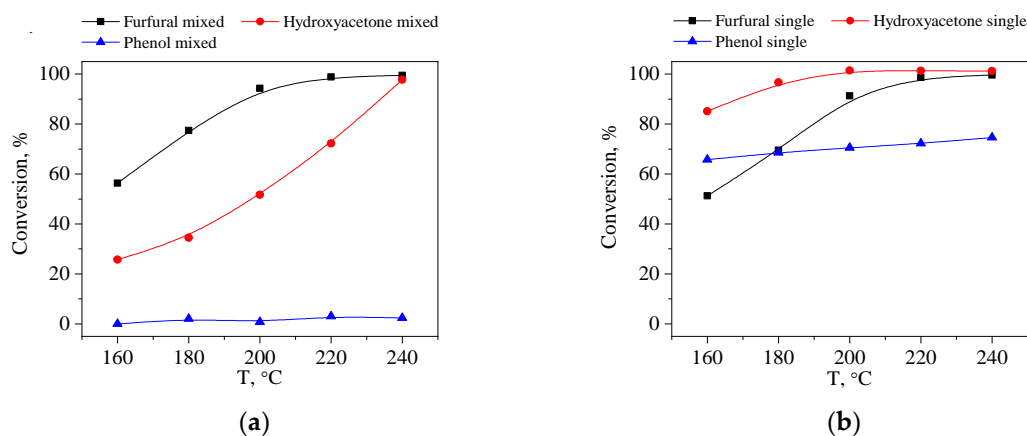

Figure 10. Effect of the reaction temperature on the conversion of furfural, hydroxyacetone, and phenol during the hydrotreatment of (**a**) mixed and (**b**) single model compounds (1 h, 3.5 MPa).

The effects of temperature on the catalytic hydrotreatment are shown in Figure 10a. Compared with the results of the hydrotreatment of the single model compound in Figure 10b, there was no significant difference in the conversion tendency for furfural with an increasing temperature. However, the differences were obvious for hydroxyacetone and phenol. During the hydrotreatment of only hydroxyacetone, it could be completely converted at 200 °C in an hour. However, it was completely transformed until the temperature was 240 °C in the hydrotreatment of mixed model compounds. In addition, phenol could not be converted in the hydrotreatment of mixed model compounds, even when the temperature rose to 240 °C, at which point the conversion was above 70% in single phenol hydrotreatment.

The effects of the reaction time are displayed in Figure 11. The reaction temperatures were set at 180 °C, which originated from the fact that the stable alcohol intermediates were converted into the by-product above 180 °C, such as the dehydration/hydrogenation of cyclohexanol into cyclohexane and furfuryl alcohol into methyl furan in the hydrotreatment of single model compounds. As exhibited in Figure 11, furfural was completely converted after 3 h. However, hydroxyacetone was completely transformed after around 10 h during the hydrotreatment of mixed model compounds, which was much slower than that of single hydroxyacetone. Besides, phenol began to be transformed after 7 h and its conversion reached 71.5% when furfural and hydroxyacetone were completely converted.
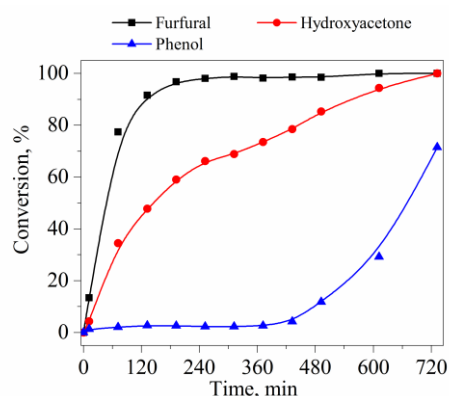
Figure 11. Effect of the reaction time on the conversion of furfuryl, hydroxyacetone, and phenol during the hydrotreatment of mixed model conversion (180 °C, 3.5 Mpa).

Therefore, it can be reasonably inferred that the conversion of hydroxyacetone and phenol was inhibited by furfural, according to the investigation of temperature and time during the hydrotreatment of mixed model compounds, especially for phenol. Besides, the conversion of phenol may also be inhibited by hydroxyacetone.

2.3.2. Exploration of the Inhibition of Phenol and Hydroxyacetone in Mixed Model Compound Hydrotreatment

In order to further investigate the reasons why phenol and hydroxyacetone hydrogenation was inhibited, different mixing conditions were studied and are presented in Table 3.

Table 3. Mixing conditions and corresponding TOF (turnover frequency) (180 °C, 1 h, 3.5 Mpa H_2 pressure).

Entry	Reactant [a]	TOF, mmol/(gcat·h)		
		Hydroxyacetone	Furfural	Phenol
1	H (1 h)	652.7	-	-
2	F (1 h)	-	361.67	-
3	P (1 h)	-	-	364.2
4	F+P (1 h)	-	240.3	2.6
5	F+P (2 h)	-	130.1	17.4
6	H+P (10 min)	1900.9	-	92.6
7	H+P (1 h)	337.5	-	57.9
8	H+F (1 h)	59.7	167.6	-
9	H+F+P (1 h)	116.4	201.6	0.00
10	H+F+P (5 h)	32.6	36.0	0.3
11 [b]	P (No.9 used catalyst, 1 h)	-	-	305.7
12 [c]	P (No.10 used catalyst, 1 h)	-	-	263.0

[a] H, F, and P represent hydroxyacetone, furfural, and phenol, respectively. [b] Catalyst used in experiment No.9 was washed three times with ethanol and dried at 80°C in air after the reaction, and was then used in experiment No.1.[c] Catalyst used in experiment No.10 was washed and dried in the same way, and then used in experiment No.12.

Experiments No.4–8 were conducted to explore the effect of the interaction between different model compounds on the hydrotreatment of them. The competition reaction between furfural and phenol was intense, as shown in No.4 and No.5. The presence of furfural had a strong inhibitory effect on the conversion of phenol, although the TOF of furfural also decreased in this situation, which can be attributed to the lower initial concentration of furfural in the mixed model compounds. As displayed in No.6 and No.7, it can be noted that hydroxyacetone also inhibited the hydrogenation of phenol, although the inhibition was weaker compared to furfural. In addition, furfural also had a strong inhibitory effect on hydroxyacetone when furfural was mixed with hydroxyacetone, as

reflected in No.8. The results of experiments No.4–8 defined the effect of the interaction among different model compounds on the hydrotreatment of them. Previous literature suggested that this may arise from the fact that the strong adsorption of furfural leads to carbon deposition on the surface of the catalyst, causing irreversible deactivation of the catalyst [59]. However, our result cannot be completely explained with this hypothesis. As shown in Figure 11, phenol began to react and was converted to 71.5% when furfural and hydroxyacetone were completely converted, which indicated that the adsorption of furfural did not cause irreversible deactivation of the catalyst at mild conditions compared to the studies conducted by Dwiatmoko et al. [59] at a relatively higher temperature, in which the conversion of guaiacol was inhibited partly because the irreversible deactivation was caused by the carbon deposition from the polymerization of adsorbed furfural and its derivatives. In addition, the results of experiments No.10 and No.11 showed that the used catalysts were still active for the hydrogenation of phenol, despite slightly decreasing, which further demonstrated that it did not mainly arise from irreversible deactivation of the catalyst and that phenol could not be converted in the initial stage of the hydrotreatment of mixed model compounds.

This arose from the fact that compared to the hydrogenation that occurred at the side chain of furfural and hydroxyacetone, the reaction of phenol occurred on the benzene ring, so more active site was necessary for phenol. Due to the small particle size of the catalyst, when the three model compounds were mixed together, the adsorption of hydroxyacetone and furfural resulted in there not being enough sites for phenol. The conversion of phenol was therefore inhibited in the hydrotreatment of mixed model compounds. The characterization of used catalysts was done to further explore the reasons why phenol could not be converted in the initial stage of the hydrotreatment of mixed model compounds.

2.3.3. Characterization and Discussion of Used Catalysts

Thermogravimetric analysis (TGA) of the reduced and used catalysts (after 5 h catalytic hydrotreatment of single or mixed model compounds) was conducted in air and an N_2 atmosphere to further determine whether there was carbon deposition in the used catalysts in Figure 12a,b and weight losses are shown in Table 4. As displayed in Figure 12a, the weight loss that TGA produced in the air atmosphere included stable carbon deposition and the carbonaceous species on the catalyst. Besides, it should be considered that the oxidation of Ni to NiO in the air could cause the weight of used catalysts to increase, as presented in Figure 12c. Therefore, the mass increase that arose from the oxidation of Ni^0 should be added to the total mass loss (M_{air}). However, as displayed in Figure 12b, the weight loss (M_{N2}) that TGA displayed in the N_2 atmosphere should just include the decomposition of the carbonaceous species on the catalyst, not the combustion of carbon deposition. The above analysis demonstrated that the mass difference between M_{air} and M_{N2} could express the amount of carbon deposition of the used catalysts, as shown in Table 4. No obvious carbon deposition on the catalyst used in the hydrotreatment of mixed model compounds was observed, which further certificated that it did not originate from the irreversible deactivation of catalysts caused by carbon deposition and that the conversion of phenol was inhibited in the initial stage of hydrogenation.
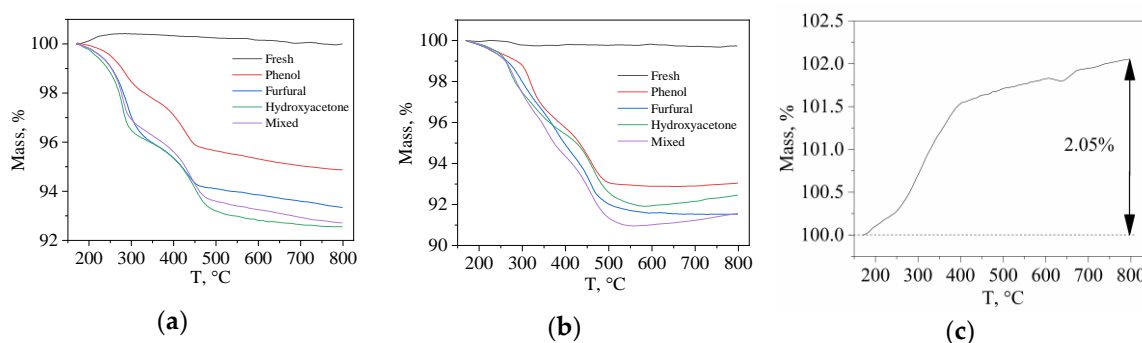
(**a**)

(**b**)

(**c**)

Figure 12. Thermogravimetric analysis (TGA) curves of the reduced and used catalyst in (**a**) air and (**b**) N_2 atmosphere, and (**c**) reduced catalyst in air after TGA analysis in N_2.

Table 4. TGA results of the reduced and used catalyst.

Samples	M [a], wt %	M_{N2} [b], wt %	M_{air} [c], wt %	Carbon Deposition, wt %
Phenol	5.1	7.1	7.4	0.3
Furfural	6.7	8.5	9.0	0.5
Hydroxyacetone	7.3	8.1	9.6	1.5
Mixed	7.5	9.0	9.8	0.7

[a] m represents the mass losses of Figure 12a; [b] M_{N2} expresses the mass losses of Figure 12b; [c] M_{air} means that m was added to the weight increase of the oxidation of Ni; Figure 12c shows that the mass gain was 2.1%. As the Ni loading amount was 8.3% according to the ICP-OES, the theoretical mass gain should be 2.3%, which matches well with the experimental results.

Ultraviolet-Raman (UV-Raman) was performed to further confirm the composition of the substances on the catalyst surface, as presented in Figure 13. The bands at 1600 and 1369 cm-1 in the four samples can be attributed to the formation of carbonaceous species formed by aromatic compounds or olefin species, rather than stable carbon deposition [60–63]. In addition, these two bands of the catalyst used in the hydrotreatment of hydroxyacetone were relatively weak, which meant that there were smaller amounts of carbonaceous species on this catalyst. This can be attributed to the relatively faster hydrogenation of hydroxyacetone. For the catalyst used in the mixed model hydrotreatment, the bands were the highest, which meant that there may be synergistic effects between phenol and furfural for the formation of carbonaceous. Sun et al., [64] studied the polymerization of sugars and phenolic compounds and found that there was cross-polymerization between the sugars or their degradation intermediates and the phenols. These synergistic effects can be used to explain the more obvious band of the catalyst used in mixed models. As the furfural was also the degradation intermediate of sugar, the presence of a carbonyl function favors carbonaceous species formation.
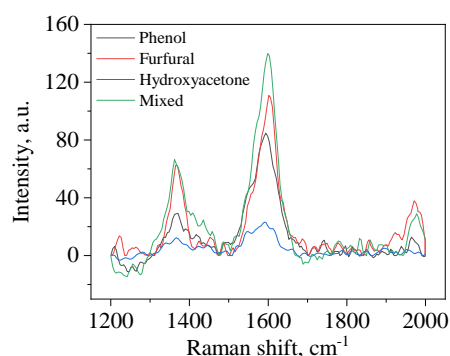

Figure 13. Ultraviolet-Raman (UV-Raman) spectra of the used catalysts.

Nitrogen adsorption–desorption isotherm measurements were taken for the used catalysts and the BET surface area results were compared with those of the reduced catalyst and are presented in Table 5. The surface areas of the used catalysts were all reduced to some degree, which can be attributed to the blockage of the pores caused by the adsorption of the carbonaceous species, which was reflected by the UV-Raman.

Table 5. BET surface area of the reduced and used catalyst.

Model Compounds	Specific Surface Area [a], m^2/g
Reduced catalyst	218.2
Phenol	198.5
Furfural	170.3
Hydroxyacetone	172.0
Mixed	180.0

[a] BET surface area.

3. Experimental Section

3.1. Materials

Phenol (99%), furfural (99%), nano fumed silica (SiO_2, 200 m^2/g, 40–70 nm, 99.8%), nickel nitrate hexahydrate (98%), and ammonium carbonate (99.999%) were purchased from Aladdin (Shanghai, China). Hydroxyacetone (95%) was purchased from Alfa Aesar (Shanghai, China); ethanol (99.8%) and isopropanol (99.9%) were purchased from Yuanli (Tianjin, China); and dodecane (98%) was purchased from Heowns (Tianjin, China). All reagents were used as received, without further pretreatment.

3.2. Catalyst Preparation

The supported Ni/SiO_2 catalyst was prepared by the deposition-precipitation method. A certain amount of $Ni(NO_3)_2 \cdot 6H_2O$ was dissolved in water to prepare 0.1 M solution of Ni^{2+} and SiO_2 was then added to the above solution in a flask while stirring. Subsequently, ammonium carbonate (the molar ratio of ammonium carbonate to Ni^{2+} was 10:1) was weighted and dissolved in water to prepare 1 M solution and then added to the above mixture while stirring. The suspension was heated to 70 °C with an oil bath and maintained for 12 h with magnetic stirring.

After that, the product was filtered and washed until the washing liquid was neutral, and then dried in air at 80 °C for 12 h. Finally, the catalyst was grinded and calcinated in a tubular furnace in air at 550 °C for 4 h (with a ramping rate of 1 °C/min from room temperature). The catalyst was reduced under pure H_2 (99.999%) at 700 °C for 2 h (with a ramping rate of 10 °C/min from room temperature) and then cooled to room temperature. To protect the catalyst from excessive oxidation, the reduced catalyst was passivated in 1% O_2/N_2 at room temperature for 3 h, before being taken out of the furnace.

3.3. Catalyst Characterization

3.3.1. Inductively Coupled Plasma Optical Emission Spectroscopy (ICP-OES)

The nickel loading amount was analysed by ICP-OES on Varian VISTA-MPX. A certain amount of catalyst was dissolved by 40% hydrofluoric acid and aqua regia for 6 h. The excess hydrofluoric acid was complexed with boric acid. After 6 h, the solution was diluted with deionized water. The measurement was repeated three times.

3.3.2. Nitrogen Adsorption–Desorption Isotherm Measurements

Porosity characterization of the reduced and used catalyst and SiO_2 support was measured by nitrogen adsorption–desorption isotherm measurements at liquid nitrogen boiling point temperature (−195.8 °C) using a Micromeritics Tristar-3000 volumetric adsorption analyzer. The SiO_2 support was

calcinated at 550 °C in air for 4 h and reduced at 700 °C for 2 h to rule out the effect of calcination and reduction on the porosity of SiO_2. Before being analysed, samples were degassed under N_2 at 100 °C for one hour and then at 300 °C for 3 h. The surface area was measured using the Brunauer−Emmett−Teller (BET) method. The pore volume and diameter were calculated from the desorption branch of the curves by the Barret–Joyner–Halenda (BJH) method.

3.3.3. H_2-Temperature Programmed Reduction (H_2-TPR)

H_2-TPR was performed in Micromeritics Auto Chem 2910 (Micromeritics Instrument Corporation, Norcross, GA, USA) equipped with a TCD detector, to determine the reduction temperature of the catalyst. A total of 50 mg of catalyst (40−60 mesh) was placed inside the U-shaped quartz tube reactor and kept at 200 °C for 60 min in argon to remove the water. Then, the system was cooled to 60 °C and the gas was converted into 10% H_2/Ar. When the baseline was stable, the system was warmed up to 780 °C at 10 °C/min and the data were recorded.

3.3.4. X-Ray Diffraction (XRD)

XRD of the reduced catalysts was performed on a Bruker D8-Focus X-ray (Bruker, Karlsruhe, Germany) diffractometer. The scanning 2Theta range was 10° to 90°, with the scan rate of 10 °/min. To investigate the change of Ni phase during the preparation, the catalysts before and after reduction were analysed by XRD.

3.3.5. X-Ray Photoelectron Spectroscopy (XPS)

XPS spectra of the catalysts after calcination and after reduction were recorded on a Kratos XSAM 800 spectrometer (Al Kα, hν = 1486.6 eV) (Kratos Analytical Ltd, Manchester, U.K.), to study the oxidation states of Ni phase on the surface. Two samples were prepared with the method mentioned in the catalyst preparation.

3.3.6. Transmission Electron Microscopy (TEM) and High-Resolution Transmission Electron Microscopy (HRTEM)

To determine the particle size and the morphology of the reduced catalyst, TEM and HRTEM were conducted on JEM-2100F (JEOL, Japan). The reduced sample was grinded and dispersed in ethanol under ultrasonic, dropped supernatant liquid on ultra-thin carbon film and dried. To reduce the error, particle size statistics were performed on more than 100 particles to obtain the average particle size and particle size distribution.

3.3.7. Thermogravimetric Analysis (TGA)

To determine the weight loss of the used catalyst, TGA was conducted with the LECO TGA701 (LECO, St. Joseph, MI, USA). A total of 10 mg of the reduced or used catalyst was loaded. The temperature was increased from room temperature to 800 °C at 5 °C/min and the data was collected during this period. To eliminate the influence of adsorbed water, the weight loss was calculated from 170 °C. N_2 and air were used as the carrier gas separately to distinguish the weight loss from carbon and organic compounds.

3.3.8. Ultraviolet (UV)-Raman

UV-Raman spectra of the reduced and used catalyst were collected with a HORIBA LabRAM HR Evolution Raman microscope (HORIBA, Kyoto, Japan) equipped with a 325 nm He-Cd ultraviolet excitation source to analyse the used catalyst.

3.4. Catalytic Hydrogenation of Biomass PL Model Compounds

Catalytic hydrotreatment experiments were performed in a 100 mL autoclave (Beijing Century SenLong experimental apparatus Co., Ltd) equipped with mechanical stirring. Phenol, furfural, hydroxyacetone, and their mixtures were chosen as model compounds. Dodecane and isopropanol were used as the internal standard substance and the solvent, respectively. When the reactant was a single model compound, 2 g model compound, 2 g dodecane, 18 g isopropanol, and 0.04 g catalyst were mixed together in the autoclave. When the reactants were mixtures of two model compounds, 1 g of each component, 1 g dodecane, 18 g isopropanol, and 0.04 g catalyst were added. When the reactants were mixtures of three model compounds, 0.7 g of each component, 0.7 g dodecane, 18 g isopropanol, and 0.04 g catalyst were introduced. After being purged with 5 MPa H_2 three times, the reactor was charged with a certain amount of H_2 and heated to reaction temperature, and then kept for a certain amount of time at a stirring speed of 500 rpm. After the reaction, the used catalyst was centrifuged and washed with ethanol and then dried at 80 °C. Each experiment was repeated twice to exclude the experimental error.

3.5. Product Analysis and Data Interpretation

Quantitative analysis was conducted by GC (gas chromatography) on the Persee GC-1100 gas chromatography apparatus (Persee, Beijing, China), which was equipped with an AT.FFAP column (30 m × 0.32 mm × 0.5 μm) and an FID (flame ionization detector). N_2 (99.999%) was used as the carrier gas. The temperatures of the injector and detector were both set at 230 °C. The programmed temperature of the oven was as follows: it was first kept at 60 °C for 4 min, and then subsequently heated to 180 °C at 5 °C/min, and to 220 °C at 10 °C/min, before finally being maintained at 220 °C for 4 min. Qualitative analysis was conducted by the Shimadzu GCMS-QP2020 gas chromatography-mass spectrometry instrument (Shimadzu, Japan) equipped with an Rtx-5MS capillary column (50 m × 0.25 mm × 0.25 μm). The temperatures of the injector and detector, and the oven, were the same as those for GC-FID mentioned above.

The following definitions of the conversion, selectivity, and yield were used in the study to quantitate the experimental result:

$$\text{Conversion}/\% = 1 - \frac{the\ moles\ of\ the\ rest\ reactant\ after\ reaction}{the\ moles\ of\ the\ initial\ reactant}, \tag{1}$$

$$\text{Selectivity}/\% = \frac{the\ moles\ of\ one\ product\ in\ all\ products}{the\ moles\ of\ all\ the\ products} \tag{2}$$

4. Conclusions

An Ni/SiO_2 catalyst was synthesized by the deposition-precipitation method and used in the mild hydrotreatment of single and mixed model compounds. Ni/SiO_2 has a narrow and small Ni particle size distribution, a remarkable mesoporous structure, and a strong metal-support interaction, which meant that unstable PL model compounds could be effectively converted into stable alcohols and mesopores could reduce the diffusion resistance of reactant molecules that had contact with active components.

During the mild hydrotreatment of single model compounds, the reaction pathways of the three substances were confirmed and further studies were conducted to improve the selectivity of stable alcohol intermediates. Furthermore, the mild hydrotreatment of mixed model compounds was conducted for a more realistic simulation of biomass PL. Furfural had an inhibitory effect on the conversion of phenol and hydroxyacetone, especially for phenol. The hydrogenation of phenol was totally suppressed initially in the hydrotreatment of mixed model compounds, while phenol began to react when the furfural was completely converted and the concentration of hydroxyacetone was low. TGA analysis indicated that the inhibition effect did not arise from the irreversible deactivation of catalysts caused by carbon deposition. UV-Raman further suggested that there were carbonaceous

species formed by substances containing a benzene ring or C=C structure, rather than carbon deposition on the catalyst surface. The findings of this work provide insights into understanding the behavior of compounds in PL during a mild catalytic hydrotreatment process. In future work, more meaningful model compounds and mixed ratios, especially molar ratios, need to be tested to simulate the PL more factually. The behavior of PL during mild hydrotreatment also needs to be clarified based on advanced characterization techniques.

Author Contributions: Investigation, D.H., A.A., T.L., and Y.Z.; methodology, W.Y.; supervision, S.X.; writing—original draft, D.H. and W.Y.; writing—review and editing, D.H., W.Y., A.A., T.L., Y.Z., and S.X. All authors have read and agreed to the published version of the manuscript.

Conflicts of Interest: The authors declare no conflicts of interest.
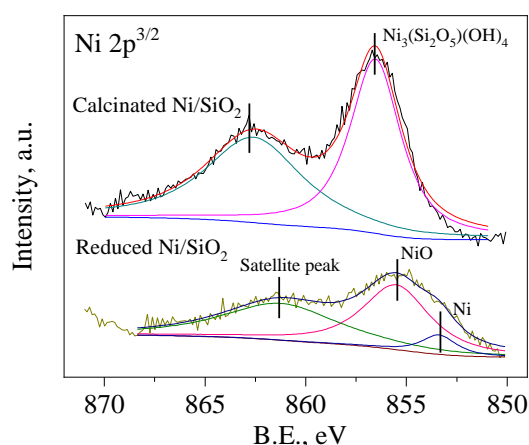
Appendix A

Figure A1. XPS spectra of the calcinated and reduced catalysts.

References

1. Panwar, N.L.; Kothari, R.; Tyagi, V. V Thermo chemical conversion of biomass—Eco friendly energy routes. *Renew. Sustain. Energy Rev.* **2012**, *16*, 1801–1816. [CrossRef]

2. Venderbosch, R.H.; Ardiyanti, A.R.; Heeres, H.J.; Yakovlev, V.; Ermakov, D.; Khromova, S.; Parmon, V.; Ermakov, D.Y.; Jakovlev, V.A.; Khromova, S.A.; et al. Hydrotreatment of Vegetal Biomass, Comprises Subjecting Vegetal Biomass to Hydrotreatment in Reactor, Where the Hydrotreatment Comprises Contacting the Biomass in Medium and Metal Oxide or Metal-Metalloid Oxide Catalyst with Hydrogen. WO2012030215-A1, 8 March 2012.

3. ŁukaszJęczmionek; Porzycka-Semczuk, K. Triglyceride zeoforming—A method for improving the low-temperature properties of second generation bio-components obtained from natural oils. *Fuel* **2013**, *113*, 17–23. [CrossRef]

4. Wang, S.; Wang, Y.; Leng, F.; Chen, J.; Qiu, K.; Zhou, J. Separation and enrichment of catechol and sugars from bio-oil aqueous phase. *Bioresources* **2016**, *11*, 1707–1720. [CrossRef]

5. Xiu, S.; Shahbazi, A. Bio-oil production and upgrading research: A review. *Renew. Sustain. Energy Rev.* **2012**, *16*, 4406–4414. [CrossRef]

6. Yin, W.; Kloekhorst, A.; Venderbosch, R.H.; Bykova, M.V.; Khromova, S.A.; Yakovlev, V.A.; Heeres, H.J. Catalytic hydrotreatment of fast pyrolysis liquids in batch and continuous set-ups using a bimetallic Ni–Cu catalyst with a high metal content. *Catal. Sci. Technol.* **2016**, *6*, 5899–5915. [CrossRef]

7. Olarte, M.V.; Zacher, A.H.; Padmaperuma, A.B.; Burton, S.D.; Job, H.M.; Lemmon, T.L.; Swita, M.S.; Rotness, L.J.; Neuenschwander, G.N.; Frye, J.G.; et al. Stabilization of Softwood-Derived Pyrolysis Oils for Continuous Bio-oil Hydroprocessing. *Top. Catal.* **2015**, *59*, 55–64. [CrossRef]

8. Cheng, S.; Wei, L.; Zhao, X.; Julson, J. Application, Deactivation, and Regeneration of Heterogeneous Catalysts in Bio-Oil Upgrading. *Catalysts* **2016**, *6*, 195. [CrossRef]

9. Baker, E.G.; Elliott, D.C. Catalytic Upgrading of Biomass Pyrolysis Oils. In *Research in Thermochemical Biomass Conversion*; Bridgwater, A.V., Kuester, J.L., Eds.; Springer: Dordrecht, The Netherlands, 1988; pp. 883–895. ISBN 978-94-009-2737-7.

10. Gagnon, J.; Kaliaguine, S. Catalytic Hydrotreatment of Vacuum Pyrolysis Oils from Wood. *Ind. Eng. Chem. Res.* **1988**, *27*, 1783–1788. [CrossRef]

11. Lee, H.; Kim, Y.M.; Lee, I.G.; Jeon, J.K.; Jung, S.C.; Do Chung, J.; Choi, W.G.; Park, Y.K. Recent advances in the catalytic hydrodeoxygenation of bio-oil. *Korean J. Chem. Eng.* **2016**, *33*, 3299–3315. [CrossRef]

12. Shu, R.; Li, R.; Lin, B.; Wang, C.; Cheng, Z.; Chen, Y. A review on the catalytic hydrodeoxygenation of lignin-derived phenolic compounds and the conversion of raw lignin to hydrocarbon liquid fuels. *Biomass Bioenergy* **2020**, *132*, 105432. [CrossRef]

13. Kim, H.; Shafaghat, H.; kon Kim, J.; Kang, B.S.; Jeon, J.K.; Jung, S.C.; Lee, I.G.; Park, Y.K. Stabilization of bio-oil over a low cost dolomite catalyst. *Korean J. Chem. Eng.* **2018**, *35*, 922–925. [CrossRef]

14. Soltes, J.; Lin, S.-C.K. Hydroprocessing of Biomass Tars for Liquid Engine Fuels. In *Progress in Biomass Conversion*; Tillman, D.A., Jahn, E.C., Eds.; Elsevier: Amsterdam, The Netherlands, 1984; Volume 5, pp. 1–68. ISBN 0192-6551.

15. Pourzolfaghar, H.; Abnisa, F.; Wan Daud, W.M.A.; Aroua, M.K. Atmospheric hydrodeoxygenation of bio-oil oxygenated model compounds: A review. *J. Anal. Appl. Pyrolysis* **2018**, *133*, 117–127. [CrossRef]

16. Elliott, D.C.; Baker, E.G. Hydrotreating Biomass Liquids to Produce Hydrocarbon Fuels. In Proceedings of the 10 Annual Symposium on Energy from Biomass and Wastes, Washington, DC, USA, 7 April 1986.

17. French, R.J.; Stunkel, J.; Black, S.; Myers, M.; Yung, M.M.; Iisa, K. Evaluate Impact of Catalyst Type on Oil Yield and Hydrogen Consumption from Mild Hydrotreating. *Energy Fuels* **2014**, *28*, 3086–3095. [CrossRef]

18. Kadarwati, S.; Oudenhoven, S.; Schagen, M.; Hu, X.; Garcia-Perez, M.; Kersten, S.; Li, C.-Z.; Westerhof, R. Polymerization and cracking during the hydrotreatment of bio-oil and heavy fractions obtained by fractional condensation using Ru/C and NiMo/Al2O3 catalyst. *J. Anal. Appl. Pyrolysis* **2016**, *118*, 136–143. [CrossRef]

19. Stankovikj, F.; Tran, C.-C.; Kaliaguine, S.; Olarte, M.V.; Garcia-Perez, M. Evolution of Functional Groups during Pyrolysis Oil Upgrading. *Energy Fuels* **2017**, *31*, 8300–8316. [CrossRef]

20. Vispute, T.P.; Huber, G.W. Production of hydrogen, alkanes and polyols by aqueous phase processing of wood-derived pyrolysis oils. *Green Chem.* **2009**, *11*, 1433. [CrossRef]

21. Sanna, A.; Vispute, T.P.; Huber, G.W. Hydrodeoxygenation of the aqueous fraction of bio-oil with Ru/C and Pt/C catalysts. *Appl. Catal. B* **2015**, *165*, 446–456. [CrossRef]

22. Kusserow, B.; Claus, P. Hydrogenation of Glucose to Sorbitol over Nickel and Ruthenium Catalysts. *Adv. Synth. Catal.* **2003**, *345*, 289–299. [CrossRef]

23. Zhang, J.; Hou, B.; Wang, A.; Li, Z.; Wang, H.; Zhang, T. Kinetic study of the competitive hydrogenation of glycolaldehyde and glucose on Ru/C with or without AMT. *AIChE J.* **2015**, *61*, 224–238. [CrossRef]

24. Luo, D.; Yin, W.; Liu, S.; Yang, N.; Xia, S.; Ma, P. Pyrolysis oil polymerization of water-soluble fraction during accelerated aging. *Fuel* **2018**, *230*, 368–375. [CrossRef]

25. Wang, H.; Male, J.; Wang, Y. Recent Advances in Hydrotreating of Pyrolysis Bio-Oil and Its Oxygen-Containing Model Compounds. *ACS Catal.* **2013**, *3*, 1047–1070. [CrossRef]

26. Zhang, X.; Tang, W.; Zhang, Q.; Wang, T.; Ma, L. Hydrodeoxygenation of lignin-derived phenoic compounds to hydrocarbon fuel over supported Ni-based catalysts. *Appl. Energy* **2018**, *227*, 73–79. [CrossRef]

27. Cheng, T.; Han, Y.; Zhang, Y.; Xu, C. Molecular composition of oxygenated compounds in fast pyrolysis bio-oil and its supercritical fluid extracts. *Fuel* **2016**, *172*, 49–57. [CrossRef]

28. Bindwal, A.B.; Bari, A.H.; Vaidya, P.D. Kinetics of low temperature aqueous-phase hydrogenation of model bio-oil compounds. *Chem. Eng. J.* **2012**, *207–208*, 725–733. [CrossRef]

29. Rodríguez-Aguado, E.; Infantes-Molina, A.; Ballesteros-Plata, D.; Cecilia, J.A.; Barroso-Martín, I.; Rodríguez-Castellón, E. Ni and Fe mixed phosphides catalysts for O-removal of a bio-oil model molecule from lignocellulosic biomass. *Mol. Catal.* **2017**, *437*, 130–139. [CrossRef]

30. Bergem, H.; Xu, R.; Brown, R.C.; Huber, G.W. Low temperature aqueous phase hydrogenation of the light oxygenate fraction of bio-oil over supported ruthenium catalysts. *Green Chem.* **2017**, *19*, 3252–3262. [CrossRef]

31. Wang, C.; Guo, Z.; Yang, Y.; Chang, J.; Borgna, A. Hydrogenation of Furfural as Model Reaction of Bio-Oil Stabilization under Mild Conditions Using Multiwalled Carbon Nanotube (MWNT)-Supported Pt Catalysts. *Ind. Eng. Chem. Res.* **2014**, *53*, 11284–11291. [CrossRef]

32. Li, H.; Li, Y.; Fang, Z.; Smith, R.L., Jr. Efficient catalytic transfer hydrogenation of biomass-based furfural to furfuryl alcohol with recycable Hf-phenylphosphonate nanohybrids. *Catal. Today* **2019**, *319*, 84–92. [CrossRef]

33. de Souza, P.M.; Rabelo-Neto, R.C.; Borges, L.E.P.; Jacobs, G.; Davis, B.H.; Resasco, D.E.; Noronha, F.B. Hydrodeoxygenation of Phenol over Pd Catalysts. Effect of Support on Reaction Mechanism and Catalyst Deactivation. *ACS Catal.* **2017**, *7*, 2058–2073. [CrossRef]

34. Prasomsri, T.; Shetty, M.; Murugappan, K.; Román-Leshkov, Y. Insights into the catalytic activity and surface modification of MoO3 during the hydrodeoxygenation of lignin-derived model compounds into aromatic hydrocarbons under low hydrogen pressures. *Energy Environ. Sci.* **2014**, *7*, 2660. [CrossRef]

35. Huynh, T.; Armbruster, U.; Kreyenschulte, C.; Nguyen, L.; Phan, B.; Nguyen, D.; Martin, A. Understanding the Performance and Stability of Supported Ni-Co-Based Catalysts in Phenol HDO. *Catalysts* **2016**, *6*, 176. [CrossRef]

36. Si, Z.; Zhang, X.; Wang, C.; Ma, L.; Dong, R. An Overview on Catalytic Hydrodeoxygenation of Pyrolysis Oil and Its Model Compounds. *Catalysts* **2017**, *7*, 169. [CrossRef]

37. Resende, K.A.; Teles, C.A.; Jacobs, G.; Davis, B.H.; Cronauer, D.C.; Kropf, A.J.; Marshall, C.L.; Hori, C.E.; Noronha, F.B. Hydrodeoxygenation of phenol over zirconia supported Pd bimetallic catalysts. The effect of second metal on catalyst performance. *Appl. Catal. B* **2018**, *232*, 213–231. [CrossRef]

38. Shi, Y.; Chen, S.; He, L.; Ning, P.; Guan, Q. Selective Conversion of Phenol in a Subcritical Water Medium Using γ-Al2O3 Supported Ni–Co Bimetallic Catalyst. *Catalysts* **2019**, *9*, 212. [CrossRef]

39. Sing, K.S.W. Reporting physisorption data for gas/solid systems with special reference to the determination of surface area and porosity. *Pure Appl. Chem.* **1985**, *57*, 603–619. [CrossRef]

40. Thommes, M.; Kaneko, K.; Neimark, A.V.; Olivier, J.P.; Rodriguez-Reinoso, F.; Rouquerol, J.; Sing, K.S.W. Physisorption of gases, with special reference to the evaluation of surface area and pore size distribution (IUPAC Technical Report). *Pure Appl. Chem.* **2015**, *87*, 1051–1069. [CrossRef]

41. Burattin, P.; Che, M.; Louis, C. Molecular Approach to the Mechanism of Deposition−Precipitation of the Ni(II) Phase on Silica. *J. Phys. Chem. B* **1998**, *102*, 2722–2732. [CrossRef]

42. Zhang, C.; Yue, H.; Huang, Z.; Li, S.; Wu, G.; Ma, X.; Gong, J. Hydrogen Production via Steam Reforming of Ethanol on Phyllosilicate-Derived Ni/SiO2: Enhanced Metal–Support Interaction and Catalytic Stability. *ACS Sustain. Chem. Eng.* **2012**, *1*, 161–173. [CrossRef]

43. Yin, W.; Venderbosch, R.H.; He, S.; Bykova, M.V.; Khromova, S.A.; Yakovlev, V.A.; Heeres, H.J. Mono-, bi-, and tri-metallic Ni-based catalysts for the catalytic hydrotreatment of pyrolysis liquids. *Biomass Convers. Biorefin.* **2017**, *7*, 361–376. [CrossRef]

44. Yang, F.; Liu, D.; Zhao, Y.; Wang, H.; Han, J.; Ge, Q.; Zhu, X. Size Dependence of Vapor Phase Hydrodeoxygenation of m-Cresol on Ni/SiO$_2$ Catalysts. *ACS Catal.* **2018**, *8*, 1672–1682. [CrossRef]

45. Sivaiah, M.V.; Petit, S.; Barrault, J.; Batiot-Dupeyrat, C.; Valange, S. CO$_2$ reforming of CH4 over Ni-containing phyllosilicates as catalyst precursors. *Catal. Today* **2010**, *157*, 397–403. [CrossRef]

46. Melo, M.A.; Airoldi, C. Energetic features of copper and lead sorption by innovative aminoalcohol-functionalized cobalt phyllosilicates. *Dalt. Trans.* **2010**, *39*, 10217–10227. [CrossRef] [PubMed]

47. Santamaria, L.; Lopez, G.; Arregi, A.; Amutio, M.; Artetxe, M.; Bilbao, J.; Olazar, M. Stability of different Ni supported catalysts in the in-line steam reforming of biomass fast pyrolysis volatiles. *Appl. Catal. B* **2019**, *242*, 109–120. [CrossRef]

48. Gong, W.; Chen, C.; Zhang, H.; Zhang, Y.; Zhang, Y.; Wang, G.; Zhao, H. Highly selective liquid-phase hydrogenation of furfural over N-doped carbon supported metallic nickel catalyst under mild conditions. *Mol. Catal.* **2017**, *429*, 51–59. [CrossRef]

49. Lorenz, P.; Finster, J.; Wendt, G.; Salyn, J.V.; Žumadilov, E.K.; Nefedov, V.I. Esca investigations of some NiO/SiO₂ and Ni-Al₂O₃/SiO₂ catalysts. *J. Electron. Spectros. Relat. Phenomena* **1979**, *16*, 267–276. [CrossRef]

50. He, J.; Lu, X.H.; Shen, Y.; Jing, R.; Nie, R.F.; Zhou, D.; Xia, Q.H. Highly selective hydrogenation of phenol to cyclohexanol over nano silica supported Ni catalysts in aqueous medium. *Mol. Catal.* **2017**, *440*, 87–95. [CrossRef]

51. Qiu, S.; Xu, Y.; Weng, Y.; Ma, L.; Wang, T. Efficient Hydrogenolysis of Guaiacol over Highly Dispersed Ni/MCM-41 Catalyst Combined with HZSM-5. *Catalysts* **2016**, *6*, 134. [CrossRef]

52. Ertl, G.L.; Hierl, R.; Knözinger, H.; Thiele, N.; Urbach, H.P. XPS study of copper aluminate catalysts. *Appl. Surf. Sci.* **1980**, *5*, 49–64. [CrossRef]

53. Xinghua, Z.; Tiejun, W.; Longlong, M.; Chuangzhi, W. Aqueous-phase catalytic process for production of pentane from furfural over nickel-based catalysts. *Fuel* **2010**, *89*, 2697–2702. [CrossRef]

54. O'Driscoll, Á.; Leahy, J.J.; Curtin, T. The influence of metal selection on catalyst activity for the liquid phase hydrogenation of furfural to furfuryl alcohol. *Catal. Today* **2017**, *279*, 194–201. [CrossRef]

55. Luna, R.; Huan, Z.; Man, Z.; Lihua, Z.; An, P.; Jiexiang, W.; Kai, Y.; Chuanqun, Z.; Suqun, X.; Hui, C.B. A highly selective and efficient Pd/Ni/Ni(OH)2/C catalyst for furfural hydrogenation at low temperatures. *Mol. Catal.* **2020**, *480*, 110639.

56. Jiménez-Gómez, C.P.; Cecilia, J.A.; Franco-Duro, F.I.; Pozo, M.; Moreno-Tost, R.; Maireles-Torres, P. Promotion effect of Ce or Zn oxides for improving furfuryl alcohol yield in the furfural hydrogenation using inexpensive Cu-based catalysts. *Mol. Catal.* **2018**, *455*, 121–131. [CrossRef]

57. Zhang, H.; Han, A.; Okumura, K.; Zhong, L.; Li, S.; Jaenicke, S.; Chuah, G.-K. Selective hydrogenation of phenol to cyclohexanone by SiO₂-supported rhodium nanoparticles under mild conditions. *J. Catal.* **2018**, *364*, 354–365. [CrossRef]

58. Ryymin, E.-M.; Honkela, M.L.; Viljava, T.-R.; Krause, A.O.I. Competitive reactions and mechanisms in the simultaneous HDO of phenol and methyl heptanoate over sulphided NiMo/γ-Al₂O₃. *Appl. Catal. A* **2010**, *389*, 114–121. [CrossRef]

59. Dwiatmoko, A.A.; Lee, S.; Ham, H.C.; Choi, J.-W.; Suh, D.J.; Ha, J.-M. Effects of Carbohydrates on the Hydrodeoxygenation of Lignin-Derived Phenolic Compounds. *ACS Catal.* **2014**, *5*, 433–437. [CrossRef]

60. Li, C.; Stair, P.C. Coke formation in zeolites studied by a new technique: Ultraviolet resonance Raman spectroscopy. *Stud. Surf. Sci. Catal.* **1997**, *105*, 599–606.

61. Tempelman, C.H.L.; Hensen, E.J.M. On the deactivation of Mo/HZSM-5 in the methane dehydroaromatization reaction. *Appl. Catal. B* **2015**, *176–177*, 731–739. [CrossRef]

62. Shin, M.; Kim, T.; Suh, Y.W. Effect of Glycerol on Coke Characteristics in the Aromatization of Aqueous Glycerol Solution. *Top. Catal.* **2017**, *60*, 658–665. [CrossRef]

63. Huang, X.; Jiao, X.; Lin, M.; Wang, K.; Jia, L.; Hou, B.; Li, D. Coke distribution determines the lifespan of a hollow Mo/HZSM-5 capsule catalyst in CH4 dehydroaromatization. *Catal. Sci. Technol.* **2018**, *8*, 5740–5749. [CrossRef]

64. Sun, K.; Xu, Q.; Shao, Y.; Zhang, L.; Liu, Q.; Zhang, S.; Wang, Y.; Hu, X. Cross-Polymerization between the Typical Sugars and Phenolic Monomers in Bio-Oil: A Model Compounds Study. *Energy Fuels* **2019**, *33*, 7480–7490. [CrossRef]